N82 23426

A numerical study of drop-on-demand ink jets

J. Fromm

International Business Machines Corporation, Research Laboratory,
5600 Cottle Road, San Jose, California 95193

Abstract

A discussion is given of ongoing work related to development and utilization of a numerical model for treating the fluid dynamics of ink jets. The model embodies the complete nonlinear, time dependent, axi-symmetric equations in finite difference form. An earlier work treated continuous jets in which periodic boundary conditions allowed study of local capillary instability to drop formation in a moving reference frame. The present study includes the jet nozzle geometry with no-slip boundary conditions and the existence of a contact circle. The contact circle is allowed some freedom of movement, but wetting of exterior surfaces has not yet been addressed. The principal objective in current numerical experiments is to determine what pressure history, in conjunction with surface forces, will lead to clean drop formation.

I. Introduction

Recent experimental fluid drop studies related to ink jet printer design have provided an extensive input to guide development of a comprehensive numerical model for treating surface tension driven flows. As a consequence, a full nonlinear model now provides feedback of fundamental interest regarding the appropriate interaction of forces for drop formation. The system of numerical programs is lengthy and complex but seems adaptable to many problems involving drops and bubbles.

In a previous study, we considered the so-called "continuous jet", where equally spaced drops are produced in a continuous stream.[1] An "infinite jet" model, assuming periodic boundary conditions for a single drop region, provided information on drop stream control through suitable harmonic disturbances. Of general interest beyond practical matters of ink jets is that these numerical solutions gave the complete intervening behavior between Rayleigh's inviscid capillary jet[2] (initial solution) and Lamb's oscillating drop after breakup[3] (final solution).

The present study has the added complication of flow from a nozzle, controlled by a pressure history intended for the release of a single drop. A contact circle is now involved with the uncertainty of what constitutes a rigorous treatment of such a boundary. Further uncertainty exists regarding the pressure history produced by a transducer, since the small scale of the jet precludes measurement of even peak pressures. Fortunately the parameter R/W (Reynolds number / Weber number) is in a range that is amenable to numerical approximation, and it therefore seems possible that numerical experimentation will shed light on the existing uncertainties.

Currently, the numerical programs are operational with contact circle treatment such that no wetting is permitted, as is generally the case with analytic treatment of pendant drops. Motion of the contact circle occurs when negative pressures (relative to ambient) are applied at the nozzle entrance and fluid is drawn inward from the free surface. Currently, a square wave history of uniform pressure at the nozzle inlet is employed to drive the jet. A positive pulse sufficient to produce the experimental drop size is followed by a negative pulse which serves to initiate detachment of a drop. The negative pulse is terminated when the net impulse returns to zero. At this stage, surface tension must carry the contraction to final detachment of the drop. The objective of the work is to establish quantitatively the conditions which provide optimum drop characteristics for high resolution printing.

In the following, we outline the numerical method which does not differ appreciably from reference 1. We then discuss a series of results which have thus far been confined to parameters of interest in ink jet hardware development. Concluding remarks point up those aspects of the work where numerical solution has provided practical insight into the behavior of the flows.

II. Numerical Method

The geometry we consider is easily visualized from an examination of output graphics of Fig. 1. A nozzle section of unit radius with inlet on the left is assumed to be connected to a cylindrical chamber with radius large compared to the nozzle. In Fig. 1 the nozzle section is five units in length. (Note that tick marks on plot axes define finite difference mesh distances). Only a small additional annular region is needed in the geometry since drops generally will be limited to sizes on the order of the nozzle diameter and wetting of the outlet facing is not currently permitted. Axi-symmetry is assumed and hence the calculation region involves only the upper half of the views in the output graphics. The lower half is added for esthetic purposes in the plotting programs.

The initial solution is impulsive with a prescribed uniform pressure at the circular cross section of the inlet. At the initial instant (t=0) the outlet meniscus is flush with the nozzle facing, this being the

equilibrium configuration in the absence of wetting. Taking the ambient pressure as zero at this free surface we begin with a linear axial pressure gradient in the nozzle section. The flow velocities are initially zero. The calculation proceeds by explicit time differences with all succeeding time steps following the same prescription which we will now outline for a first step.

Because we here use a vorticity streamfunction formulation our first aim is to provide appropriate boundary conditions for the latter. This is rather complex since indeed none of the boundaries except the axis of symmetry can be treated simply especially since we want a time varying pressure at the inlet and also wish to provide for entrance flow from a chamber. We begin in a somewhat roundabout way by computing the velocity fields through the momentum equations. In axi-symmetric form these equations are

$$\frac{\partial u}{\partial t} + \frac{\partial u^2}{\partial z} + \frac{1}{r}\frac{\partial uvr}{\partial r} = -\frac{\partial P/\rho}{\partial z} - \frac{\nu}{r}\frac{\partial}{\partial r}(\omega r)$$

$$\frac{\partial v}{\partial t} + \frac{\partial uv}{\partial z} + \frac{1}{r}\frac{\partial v^2 r}{\partial r} = -\frac{\partial P/\rho}{\partial r} + \nu\frac{\partial \omega}{\partial z}\,. \qquad (1)$$

Here u is the axial velocity (z direction) and v is the radial velocity (r direction). P is the pressure, ρ is the fluid density and ν the fluid viscosity. We choose to express the diffusion terms as vorticity gradients because the vorticity (ω) is always available to simplify the calculation. However, we currently are expressing the diffusion in the axial velocity equation in terms of u because accuracy in the nozzle boundary layer seems to require it.

A small forward integration in time of (1) leads to flow because of the pressure gradient in the nozzle. Now by integrating the first of (1) over a fluid (control) volume of the nozzle we may obtain the uniform streamfunction value at the nozzle boundary relative to a zero streamline at the axis. That is, the time derivative of the streamfunction Q at the nozzle surface becomes

$$\left(\frac{dQ}{dt}\right)_{r_o} = \frac{1}{z_o}\int_o^{r_o} r(u_L^2 - u_R^2 + P_L - P_R)dr - \frac{\nu r_o}{z_o}\int_o^{r_o} \omega_{r_o} dz \qquad (2)$$

where we have deleted terms that do not contribute. In (2) L and R refer to left and right cross sections of the cylindrical control volume which initially includes the entire fluid region. z_o is the length of the nozzle and r_o its radius.

We can, of course, have the control volume continue to be all of the fluid region even when a drop is forming but then (2) becomes a more difficult expression. Also, if the free surface draws inward the control volume, as expressed in (2), must be shortened by revising z_o and excluding some of the fluid near the outer edge of the outlet.

Thus far we still do not know the boundary conditions for Q at the entrance of the nozzle or at the free surface. For the latter we integrate the expressions

$$\frac{\partial Q}{\partial z} = -rv \quad \text{and} \quad \frac{\partial Q}{\partial r} = ru \qquad (3)$$

singly or in combination, beginning at the axis of symmetry outward to the surface. This provides for Q at points on the surface at roughly mesh length distances. It is necessary, however, to define the free surface as a set of particles generally 5 to 10 per mesh distance. At these surface particles Q is given through interpolation among those given above and the value previously obtained at the nozzle boundary.

Finally, two conditions are provided at the inlet. If flow is inward we simulate flow from a large chamber by requiring uniform inflow. This effectively requires the boundary layer at the nozzle surface to begin at the inlet. With Q already known at the nozzle boundary, a mean velocity u may be obtained using the second of (3) for the entire inlet cross section. Reversing the procedure we obtain Q at inlet mesh points. Q is not linear in the axis-symmetric case.

For reverse flow we assume that flow into the chamber will be the same as in the immediately adjacent region inside the nozzle or

$$\frac{\partial Q}{\partial z} = 0$$

there.

At this point we are not yet ready to solve internal streamfunction values, we need yet to know the vorticity in the interior. Using the time dependent equation

$$\frac{\partial \omega}{\partial t} + \frac{\partial u\omega}{\partial z} + \frac{\partial v\omega}{\partial r} = \nu \left[\frac{\partial^2 \omega}{\partial z^2} + \frac{\partial}{\partial r} \left(\frac{1}{r} \frac{\partial \omega r}{\partial r} \right) \right] \tag{4}$$

we increment the vorticity forward in time as we had done the velocities. This is of course meaningless for the first time step because the vorticity field is null. At the second time step and all following vorticity will derive from the no-slip nozzle surface and to a lesser extent from the free surface.

Internal streamfunction values are now obtained by simultaneous solution at all net points of the equation

$$\frac{\partial^2 Q}{\partial z^2} + r \frac{\partial}{\partial r} \left(\frac{1}{r} \frac{\partial Q}{\partial r} \right) = -r\omega \ . \tag{5}$$

This is followed by resetting the velocities using (3) and the after thought determination of vorticity at the nozzle surface using

$$\omega_b = - \left(\frac{\partial u}{\partial r} \right)_b$$

The redundancy of the above may be questioned but our objective thus far is to provide for more options on how solution is to be carried out both for convenience and accuracy. Solution of (5) is of necessity by iteration rather than direct because of the time varying fluid region. Convergence is of course enhanced if in the course of getting surface streamfunction values through (3) one fills in internal points. The difference in the final outcome from (5) relates to truncation errors in (3), particularly in the nonlinear terms. One in fact would find that strict use of (3) only would leave in doubt what value to give the streamfunction at the nozzle surface because each integration upward along z=constant lines would give a different error.

With the streamfunction given at "Lagrangian" free surface points we may evaluate the normal and tangential velocities there. That is

$$u_\tau = \frac{1}{r} \frac{\partial Q}{\partial \eta} \quad \text{and} \quad u_\eta = - \frac{1}{r} \frac{\partial Q}{\partial} \tag{6}$$

where τ is tangential and η is normal. The second of these is readily obtained from particle Q values, the first through a nearest approach method relative to selected interior points followed by interpolation. We require surface points or particles to carry with them coordinate information, local are lengths and angles (relative to the axis of symmetry). Using the angle we may obtain u and v for the particles through a rotational transformation.

Updating the surface configuration with

$$\frac{dz}{dt} = u \quad \text{and} \quad \frac{dr}{dt} = v \ , \tag{7}$$

we proceed to determine new local arc lengths along the surface and new angles. Thus

$$\delta\tau^2 = \delta z^2 + \delta r^2$$

and

$$\alpha = \tan^{-1} \frac{\delta r}{\delta z} \ . \tag{8}$$

It is now easy to obtain surface pressures. Relative to ambient "zero" pressure they are given by

$$\left(\frac{P}{\rho} \right)_s = \sigma \left(\frac{\cos \alpha}{r} - \frac{\partial \alpha}{\partial \tau} \right) + \nu \frac{\partial u_\eta}{\partial \eta} \ , \tag{9}$$

where σ is the surface tension coefficient. The first term on the right expresses the destabilizing curvature around the axis of symmetry, the second, the stabilizing curvature in the r-z plane and the last term the pressure contribution from local deformation. For the last term we again use a closest approach method for evaluation relative to selected interior points. However, a local continuity expression

$$\frac{\partial u_\eta}{\partial \eta} + \frac{\partial u_\tau}{\partial \tau} - u_\eta \frac{\partial \alpha}{\partial \tau} + \frac{v}{r} = 0 \tag{10}$$

could probably be used.

At this stage we may iterate a Poisson's equation for the pressure. That is

$$\frac{\partial^2 P/\rho}{\partial z^2} + \frac{1}{r}\frac{\partial}{\partial r}\left(r\frac{\partial P/\rho}{\partial r}\right) = -G \tag{11}$$

where

$$G = \frac{\partial^2 u^2}{\partial z^2} + \frac{2}{r}\frac{\partial uvr}{\partial r \partial z} + \frac{1}{r}\frac{\partial v^2 r}{\partial r} . \tag{12}$$

The boundary condition for the pressure is known everywhere except at the nozzle surface where the condition on the derivative is

$$\left(\frac{\partial P}{\partial r}\right)_b = \nu\left(\frac{\partial \omega}{\partial z}\right)_b . \tag{13}$$

G is required at only interior points.

Obtaining the vorticity at the free surface has been somewhat of a problem. In terms of surface quantities we write

$$\omega = \frac{\partial u_\eta}{\partial \tau} + \frac{\partial u_\tau}{\partial_\eta} + u_\tau \frac{\partial \alpha}{\partial \tau} . \tag{14}$$

Unfortunately in a stationary reference frame this is subject to large errors because in a spherical drop (for example) large numbers must effectively cancel to produce a small real vorticity. To overcome this we define velocities relative to a mean for each contiguous part of the fluid so that (14) is evaluated in terms of disturbance quantities.

Scaling to permit nondimensional calculation is the same as with the earlier capillary instability problem.[1] The reference length is the nozzle radius r_o. The reference velocity is the capillary wave velocity

$$v_o = \left(\frac{\sigma}{\rho r}\right)^{1/2} , \tag{15}$$

giving a time scale

$$t_o = \left(\frac{\rho r^3}{\sigma}\right)^{1/2} . \tag{16}$$

This leads to use of the single parameter, Reynolds number over Weber number

$$\frac{R}{W} = \left(\frac{\sigma r}{\rho v^2}\right)^{1/2} . \tag{17}$$

Thus the above equations are made dimensionless by replacing ν by W/R wherever it appears and replacing σ by 1.0.

III. Results

During the development of the numerical program there was constant reference to experimental work that was being conducted in the development of ink jet hardware.[4] Unfortunately because of the small size of the jet the crucial measurement of driving pressure could not be made. Lacking this knowledge, along with uncertainty concerning the numerical program itself, made convergence to a successful method very difficult. A failure to obtain a solution comparable to experiment could mean being outside the range of pressure values appropriate for drop formation or could mean there was a fundamental problem in the numerical program. The program is quite complex and the running times are by no means short. Unlike experiments which can be conducted in rapid succession to achieve a certain operating behavior, the numerical experiments took too much time for many wrong guesses. Now, however, we are quite close to experiment and the model has shown evidence of being adequate. We will perhaps never know the exact character of the pressure that drives the jet but once having achieved agreement in jet characteristics, here demonstrated in a quantitative visual form, we are in a

position to understand most properties of interest in the flows. Even now, however, one must be mindful of limitations of the approximate solution since unlimited grid resolution is of course impossible.

To illustrate the numerical solutions we have chosen a case which gives the most interesting overall results achieved by the time of this writing. Figures 1, 2 and 3 show a sequence of four solutions each in consecutive times for R/W=5. The pressure history is one which begins with a suction (negative pressure) followed by a positive pressure and then a negative pressure again. The second negative pressure terminates when the net impulse is zero. While not necessary, a very small residual positive pressure rather than zero was maintained for the remainder of the running time of this case. The square wave pressure at the inlet and times (both in nondimensional units) are as in Table 1.

Table 1

t	P/ρ
0 - 0.21	-60.0
0.21 - 0.82	+80.0
0.82 - 1.43	60.0
1.43 -	+ 1.0

The nondimensional times for the plots illustrated are given in Table 2.

Table 2

Fig.	Time	Plot Interval Q	QMAX	QMIN	Plot Interval P	PMAX	PMIN
1-1	0.25	0.03125	0.0	-0.52	4.0	80.0	-2.9
1-2	0.68	0.125	2.03	0.00	4.0	93.3	0.2
1-3	1.03	0.0625	1.97	0.00	4.0	7.5	-84.0
1-4	1.64	0.0625	0.99	-0.17	0.5	7.1	-3.0
2-1	2.05	0.03125	0.78	-0.08	0.25	4.5	-0.4
2-2	2.52	0.03125	0.66	-0.07	0.25	4.2	0.0
2-3	2.97	0.03125	0.60	-0.06	0.125	4.2	0.7
2-4	3.57	0.03125	0.53	-0.05	0.25	7.6	0.0
3-1	4.18	0.03125	0.53	-0.05	1.0	17.1	-1.2
3-2	4.52	0.03125	0.53	-0.05	1.0	20.7	-0.4
3-3	4.67	0.03125	0.54	-0.05	2.0	48.6	0.6
3-4	5.03	0.03125	0.52	-0.03	2.0	35.9	0.6

In all figures the streamfunction is plotted as solid lines. Negative streamlines include tick marks. This is manifested as tick marked lines for flow to the left (reverse flow in the nozzle) where the boundary layer vorticity is predominantly negative. The vorticity vector (positive) is outward in upper half plane and inward in the lower half. The center line is the streamline Q=0 as discussed previously. Where this line appears it is a solid line without tick marks. There are also tick marks on the solid boundaries of the nozzle but since these are rectilinear they are distinguishable from streamlines. As mentioned before, the tick mark spacing on the rectilinear lines show the grid spacing. This is only roughly true on curved streamlines.

Pressure "isobars" are plotted as dashed lines with shorter dashes for negative pressures. The zero pressure line also has long dashes.

One can use the above information and Table 2 to determine contour values throughout the plots. In some places this is difficult but knowing the maximum and minimum values helps and greater detail is probably of little use. Because of limited plotting area, say in the contracted neck of the jet, the isobars are difficult to distinguish as negative or positive. They are of course positive there because of the high surface pressure. Also it should be noted that in the axi-symmetric case streamlines are not uniformly spaced for a uniform flow velocity. This is the reason for the gap in streamlines along the central axis where a tube of flow involves little true flow because its cross sectional area is small, yet the flow velocity may be high.

Beginning with Fig. 1 and referring to Table 1 we note that the time is in the period where the inlet pressure is positive but flow is still into the chamber because of fluid inertia from the initial suction period. The left most isobar at the inlet is +80 (see Table 2) while the lowest pressure is at the concave meniscus surface and is -2.9. As a reference it is of interest that, in nondimensional units, a drop of unit radius has a surface pressure of +2.0. One unit of pressure being being provided by each component of the surface tension. Here in the first plot the stable component of the surface tension is such as to restore the

flush status of the meniscus at the face of the nozzle. Acting along with the positive inlet pressure the flow direction is soon reversed.

In the second plot of Fig. 1 the toroidal circulation at the inlet is because of fl v bending inward from the simulated large chamber preceding the nozzle. The pressure is negative at points just inward from the circulation where the flow rate is high while at the center line the deformation causes a pressure exceeding the inlet pressure. The meniscus surface has a pressure near unity.

In the next plot a drop is forming through forward motion even though the inlet pressure has been reversed. Note the short dashed lines of pressure (negative) and a zero pressure in the contracted region of the incipient drop. Again the inlet toroidal circulation is still producing a pressure lower than the applied inlet pressure but now more negative than the -60 units there. The circulation is in the process of spreading and dieing out.

In the last plot of Fig. 1 only remnants of the inlet circulation remains and a separation streamline now divides flow forward in the drop with predominantly reversed flow in the nozzle. Note that reversed flow begins in the boundary layer of the nozzle. At the time of the last plot of Fig. 1 the pressure cycle is past. The remaining motion of the jet is passive except for the minor influence of the small positive (unit pressure) hereafter present at the inlet. The highest pressure is at the forward most point of the jet and is a result of local deformations only.

In Fig. 2 the progress of the jet is observed at four succeeding stages. In the first of these there is evidence of local reverse circulation at the meniscus region tending to remove the concave curvature. This and the continuing flow into the chamber are because of the stabilizing surface tension in this region. At the same time the destabilizing surface tension component is causing higher pressures at the contraction although at this stage contraction is dominated simply by mass depletion due to the forward and backward flow. These processes continue to the time of the last plot of Fig. 2 where the surface tension pressure at the contraction is becoming an influence on local behavior. The meniscus region has been pushed outward to be convex partly because of the local high pressure and partly from inertial motion from the earlier restoring pressure. Also the taper of the connecting shank to the drop is no longer linear. This further indicates the influence of the surface tension pressure at the contraction.

In Fig. 3 we continue toward drop break off and include two plots following breakoff. Note that a restoring pressure of the meniscus portion drives fluid into the chamber to a small extent so that the outward bulge is diminished between the first and second plot of Fig. 3. Also we note that a second contraction is occurring just behind the drop.

Drop break off was here preset to occur when only one mesh distance (1/20 of the nozzle diameter) remained. At this point the mechanics of the numerical program requires a zero radius and local angles consistent with a break. The break is assumed to be locally spherical so that the two components of surface tension are the same. This eliminates the singularity of the unstable component which takes on the value of the stabilizing component.

Two separate problems are solved simultaneously after breakup. The meniscus converges here to a spherical surface of unit radius because of the residual unit pressure at the inlet. The drop portion of the jet proceeds toward a state where a drop plus a satellite exist because of the contraction behind the main drop.

IV. Concluding Comments

We are interested here in summarizing those things learned from the numerical model thus far. In some cases the information was partially known from experiment and matters were clarified and/or confirmed by the model. In other cases the information from the model gave insight thus far unobtainable experimentally.

1. The peak pressure magnitudes for driving the jet are now obtainable. These, of course, depend on nozzle losses but can be fairly well estimated for an initial trial calculation.

2. The pressure history to drive the jet is nearly a symmetric one for clean drop formation with a net zero impulse for a single drop. The negative phase of the pressure history is essential to drop break off in the range of parameters here studied.

3. Uniform pressure at the inlet cross section and ignored wetting of the outer facing of the nozzle are reasonable simplifying assumptions that do not affect comparison with experiment.

4. In the range of parameters here studied, the meniscus is very overdamped as is the drop. Experimental meniscus oscillations presumably relate to chamber or chamber to nozzle transition characteristics. The latter can be studied with the present model.

5. The flow fields throughout the history of drop generation may be analyzed in almost complete detail from the numerical results and, internal flows, usually not visible experimentally, may here be studied.

References

1. Fromm, J. E., "Finite Difference Computation of the Capillary Jet, Free Surface Problem," Lecture Notes in Physics 141, 188-193, Seventh International Conference on Numerical Methods in Fluid Dynamics, Springer-Verlag, Berlin 1981.
2. Rayleigh, J. W. S., The Theory of Sound, Vol. 2, p. 351, Dover. 1945.
3. Lamb, H., Hydrodynamics, p. 450, Dover. 1945.
4. Lee, F. C., Mills, R. N., Falke, F.E., "Drop-on-Demand Ink Jet Printing at High Print Rates and High Resolution," to be published.

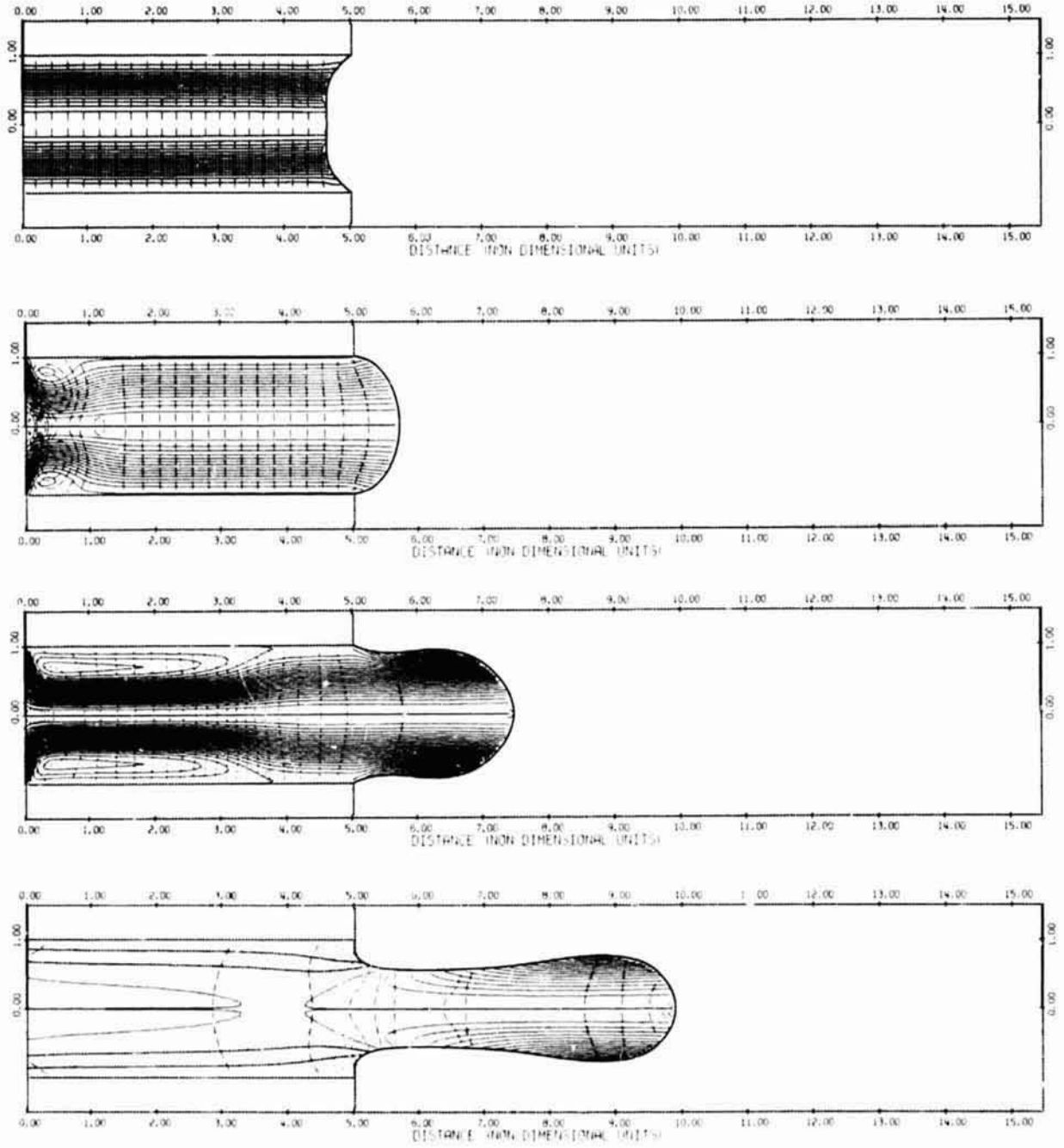

Figure 1. Computer graphical output for numerical solution of jet drop formation. See Table 2.

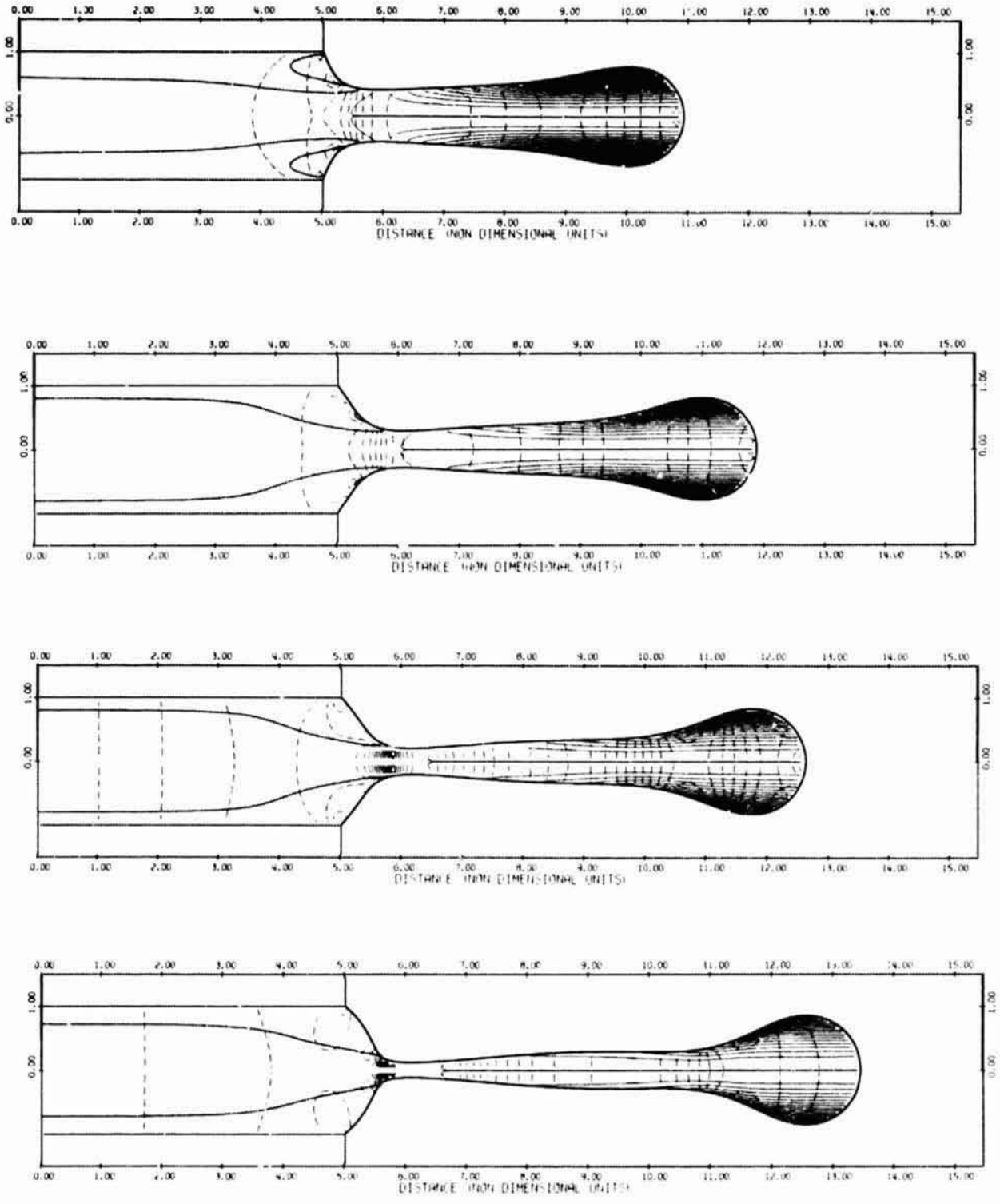

Figure 2. Continuation of Fig. 1.

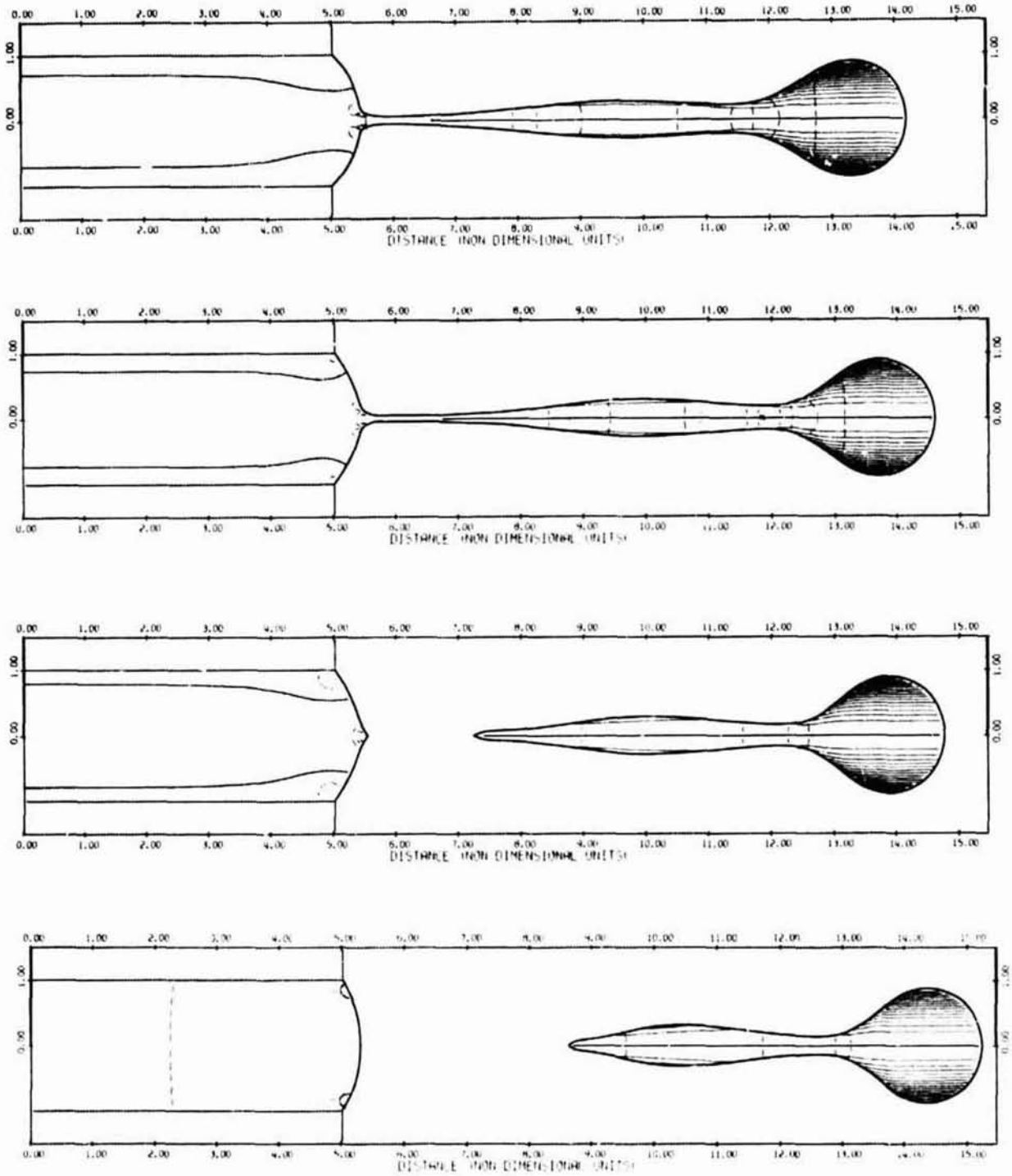

Figure 3. Continuation of Fig. 1.